

## Article

# Experimental Study on Dynamic Characteristics of Saturated Soft Clay with Sand Interlayer under Unidirectional and Bidirectional Vibration

Sui Wang <sup>1,2,3,\*</sup>, Yuanqiang Cai <sup>1</sup>, Liyong Zhang <sup>2</sup>, Yongjian Pan <sup>2</sup>, Bin Chen <sup>3</sup>, Peng Zhao <sup>3</sup> and Yuanming Fang <sup>3</sup><sup>1</sup> College of Civil Engineering, Zhejiang University of Technology, Hangzhou 310014, China; caiyq@zju.edu.cn<sup>2</sup> Zhejiang Engineering Survey and Design Institute Group Co., Ltd., Ningbo 315012, China; lyzhang111@126.com (L.Z.); pyjwj1963@163.com (Y.P.)<sup>3</sup> School of Civil and Transportation Engineering, Ningbo University of Technology, Ningbo 315211, China; chenbin@nbut.edu.cn (B.C.); zhaopeng02022@163.com (P.Z.); fym\_1999@163.com (Y.F.)

\* Correspondence: wangsui10610@163.com

**Abstract:** The marine and alluvial plains along the southeastern coast of China are widely distributed in sandy formations, including smaller sand lenses and interlayers. The interlayers of sand have a significant impact on the mechanical properties of soft clay. In this paper, a large number of undrained unidirectional and bidirectional cyclic loading tests for soft clay with sand interlayers were carried out by a dynamic triaxial test system. Test results show that, under unidirectional and bidirectional cyclic vibration, the area of the hysteresis loop decreases and the slope of the connecting line at both ends of the hysteresis loop increases with the increasing of frequency. For the same vibration frequency, the area of the bidirectional vibration hysteresis loop and the slope of the connecting line at both ends are smaller than that of the unidirectional cyclic vibration. Under the same dynamic stress ratio, cumulative axial deformation caused by unidirectional and bidirectional vibration increases with the increasing frequency. Under unidirectional vibration, dynamic elastic modulus decreases at first, and then increases with the increasing frequency. For the same frequency, dynamic elastic modulus of the sample increases with the increase in cycles. Due to the effect of radial cyclic stress, the curves of dynamic elastic modulus and damping ratio with frequency under bidirectional vibration are opposite to those under unidirectional vibration.

**Keywords:** soft clay; sand interlayer; unidirectional and bidirectional vibration; cyclic stress ratio; vibration frequency; cumulative deformation



**Citation:** Wang, S.; Cai, Y.; Zhang, L.; Pan, Y.; Chen, B.; Zhao, P.; Fang, Y. Experimental Study on Dynamic Characteristics of Saturated Soft Clay with Sand Interlayer under Unidirectional and Bidirectional Vibration. *Buildings* **2023**, *13*, 2534. <https://doi.org/10.3390/buildings13102534>

Academic Editor: Syed Minhaj Saleem Kazmi

Received: 8 August 2023

Revised: 1 September 2023

Accepted: 26 September 2023

Published: 7 October 2023



**Copyright:** © 2023 by the authors. Licensee MDPI, Basel, Switzerland. This article is an open access article distributed under the terms and conditions of the Creative Commons Attribution (CC BY) license (<https://creativecommons.org/licenses/by/4.0/>).

## 1. Introduction

Soft clay is a special soil mass formed by marine and lacustrine sediments in coastal, lake, swamp, and river bay areas in modern times. It is generally characterized by high water content, high compressibility, low strength, poor permeability, and high sensitivity and rheology [1–7]. According to the survey results of Ningbo metro, a large number of loose sand interlayer with a thickness of about 10cm are in the soft clay of metro tunnel engineering. According to the design code, this kind of interlayer has almost no influence on the evaluation of foundation liquefaction, but on the other hand, its foundation liquefaction can cause dramatic changes in stratum deformation, which will cause the subway tunnel to bear an additional huge horizontal thrust and cause damage to the subway tunnel. In the previous seismic response analysis, it is considered that the seismic action is mainly horizontal shear. The stress condition is mainly simulated by the stress on the 45° plane of the soil element under the condition of uniform consolidation under the cyclic load of unidirectional excitation. Yasuhara [8] and Matsui [9] have conducted in-depth research on the strength and stiffness attenuation of soil after cyclic loading, and pointed out the influence of cyclic cycles. Moreover, in terms of material constitutive model representation,

scientific publications have proposed yield functions that represent very reliably the cyclic behavior of clays [10,11]. To sum up, only the effect of horizontal shear is considered in the seismic design, which is not safe for the actual project, and the effect of vertical seismic load should also be considered.

A large number of tests have been carried out on the dynamic characteristics of soft clay under cyclic loading at home and abroad. In the 1960s, Seed and Lee [12] proposed that the action of seismic wave can be simplified as the action of applying equivalent reciprocating horizontal shear stress to the soil under the condition that the vertical stress remains unchanged. Wichtmann [13] considered the dynamic characteristics of soil under the coupling action of vertical cyclic normal stress and horizontal cyclic normal stress under traffic load, which confirmed that the existence of horizontal cyclic normal stress greatly affected the dynamic characteristics of soil; under unidirectional vibration, the pore pressure and deformation of the specimen accumulated more rapidly, and thus the failure was reached earlier. Kammerer [14] studied the pore pressure characteristics of saturated sand under bidirectional vibration, and the results showed that the influence of bidirectional vibration on the dynamic pore pressure was significantly greater than that of unidirectional vibration, and the dynamic pore pressure changed more greatly under bidirectional vibration. Hyde [15] conducted a series of cyclic undrained tests on silty clay samples. The test results show that cyclic loading on normal and weakly overconsolidated soils will cause a significant increase in overconsolidation. The research results of Silvestri [16] and Narasimha [17] show that the effective consolidation pressure, deformation, and undrained strength of clay under cyclic loading are affected by the loading frequency. Liang [18] proposed a constitutive model of saturated soft clay under dynamic load based on the concept of boundary surface plasticity and considering the anisotropy of materials by using the node invariants of second-order stress tensor and clay structure tensor. However, there is no relevant research on the dynamic characteristics of saturated soft clay with interlayer sand under the condition of bi-directional excitation cyclic load.

Therefore, in this paper, a bidirectional dynamic triaxial test system was used to carry out bidirectional excited cyclic vibrations under different radial cyclic stress ratios, different frequencies, and different waveforms on the undisturbed soft clay with a sand interlayer in the Ningbo metro excavation; the influence of interlayer sand was analyzed on the dynamic characteristics of saturated soft clay.

## 2. Research Contents and Methods

### 2.1. Sample Equipment and Materials

A British GDS (Global Digital System) bidirectional dynamic triaxial test system was adopted, as shown in Figure 1. During the test, GDS-LAB software v2.6.7 in the computer could collect the stress, strain, pore pressure, and other data during the vibration of the sample.



(a) Dynamic confining pressure and servo motor (b) Pressure control system diagram machine

**Figure 1.** GDS bidirectional dynamic triaxial test system.

**Preparation of undisturbed soil sample:** The undisturbed soil is cut into  $\Phi \times H = 38 \text{ mm} \times 76 \text{ mm}$  soil samples according to the specifications, as shown in Figure 2. Since the soil sample is composed of soft clay and a large number of sand interlayer with small thickness inside, it is necessary to avoid delamination of the soil sample and failure of cutting. The basic physical parameters of soil samples are shown in Table 1.



**Figure 2.** Soft clay sample with intercalated sand. (Taken from Binjiang Waterfront Project, No. zk167-02, 515-518).

**Table 1.** Basic physical parameters of soil sample.

Property	Value
Density $\rho / (\text{g} \cdot \text{cm}^{-3})$	1.82
Plastic limit $I_p$	15.6
Liquid limit $w_L / \%$	40.1
Dry density $\rho_d / (\text{g} \cdot \text{cm}^{-3})$	1.36
Moisture content $\omega / \%$	34.22
Cohesion $c$ (kPa)	19.5
Internal friction angle $\varphi$ ( $^\circ$ )	29.74

The sample soil is taken from the undisturbed soil in the Ningbo metro excavation, Zhejiang Province, and the depth of the soil sample is 15–20 m. Interlayer sand soft clay is grayish yellow, soil is soft, and has a rotten smell. Among them, the interlayer sand is fine and smooth. The basic physical parameters of soil samples are shown in Table 1.

## 2.2. Comparison of Single and Bidirectional Test Principles

A uniaxial excitation cyclic triaxial test keeps the lateral confining pressure unchanged, and apply  $\pm\sigma_d/2$ ; therefore, the cyclic shear stress applied to the  $45^\circ$  inclined plane of the specimen is still  $\pm\sigma_d/2$ ; however, the normal stress becomes  $\sigma_0 \pm \sigma_d/2$ , as shown in Figure 3.

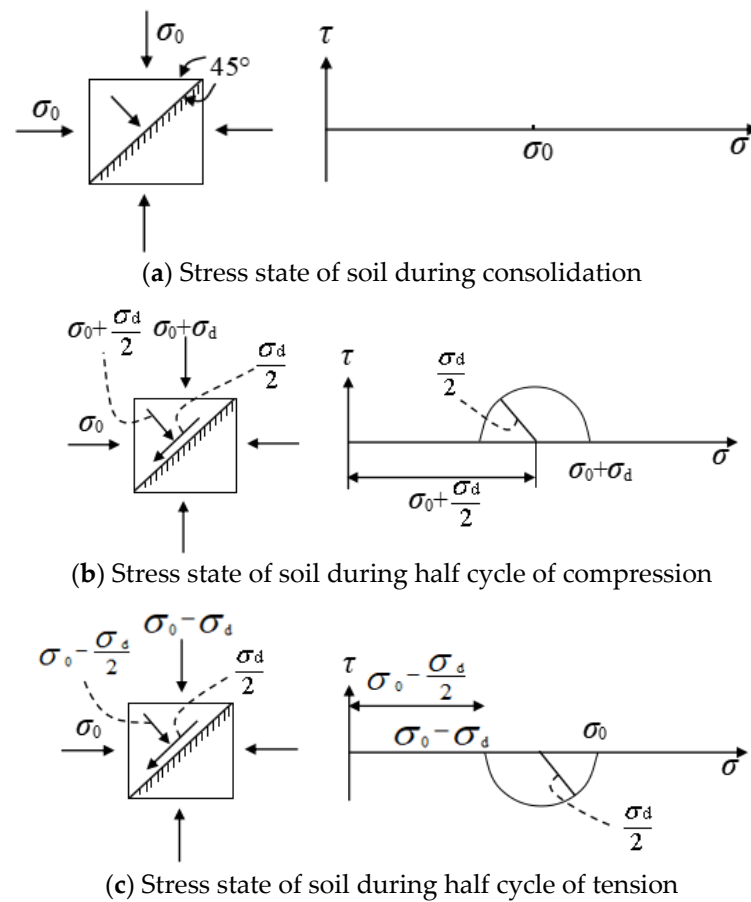


**Figure 3.** The principle of unidirectional test.

The biaxial excitation cyclic triaxial test is to apply  $\pm\sigma_d/2$  cyclic stress of, and  $\mp\sigma_d/2$  cyclic stress; therefore, the normal stress on the  $45^\circ$  plane of the specimen remains unchanged to simulate the stress state of soil level during earthquake. The test principle is shown in Figure 4.

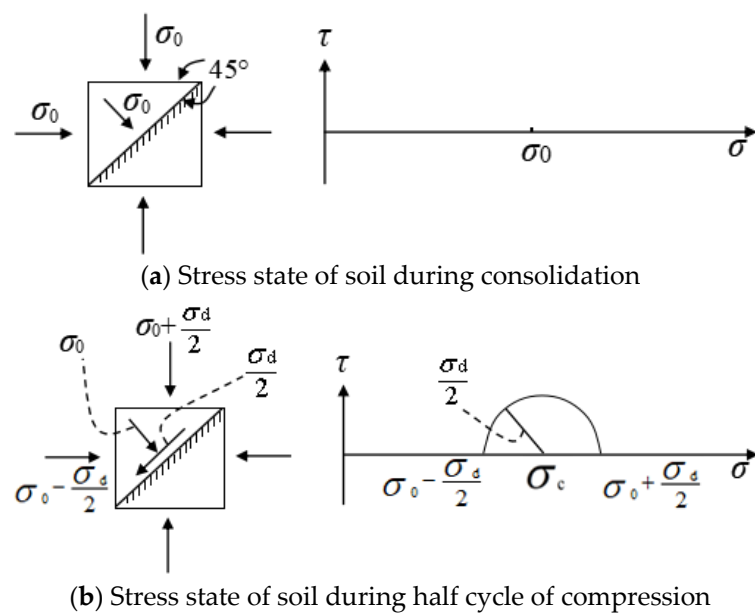


**Figure 4.** Cont.

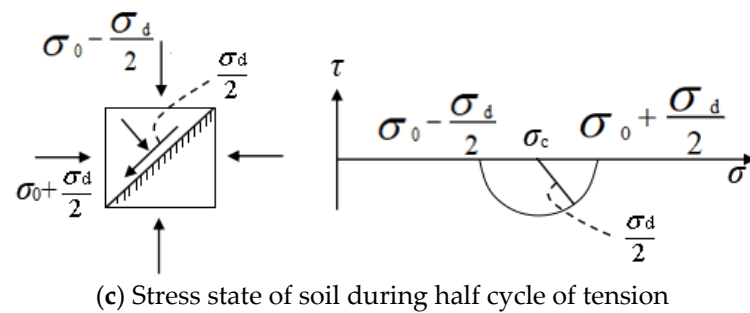


Figure 4. The principle of bidirectional test.

### 2.3. Test Method

(1) Sample preparation: Undisturbed samples with a diameter of 38 mm and a height of 76 mm are used in the test. The samples are prepared according to the soil test specification.

(2) Saturation stage: The samples are put into the vacuum saturator to vacuum. When the vacuum pressure is exposed to negative pressure, maintain the vacuum pressure in the cylinder for more than 1 h and stand for more than 10 h. In order to ensure that the saturation reaches more than 95%, the samples are saturated by back pressure before the experiment until the saturation meets the requirements [19].

(3) Consolidation stage: isobaric consolidation is adopted in the test, and the consolidation confining pressure is 100 kPa.

(4) Vibration stage: The loading mode of stress control is adopted. The loading waveform is generated by the servo system, and different waveforms can be imported through the test system. The detailed test scheme is shown in Table 2.

Table 2. Scheme of dynamic triaxial test.

ID	Frequency $f/\text{Hz}$	Confining Pressure $\sigma'_3/\text{kPa}$	$r_c$	$R_c$	N
D-1	0.2	100	0.1	0	10,000
D-2	0.5	100	0.1	0	10,000
D-3	1.0	100	0.1	0	10,000
D-4	2	100	0.1	0	10,000
D-5	5	100	0.1	0	10,000
S-1	0.2	100	0.1	0.05	10,000
S-2	0.5	100	0.1	0.05	10,000
S-3	1.0	100	0.1	0.05	10,000

In this test, the GDS bidirectional dynamic triaxial test system is adopted to carry out experimental research on dynamic deformation characteristics of saturated intercalated sand soft clay. In order to measure the stress level of cyclic axial eccentric stress and cyclic confining pressure, the axial cyclic stress ratio  $r_c$  and radial cyclic stress ratio  $R_c$  are introduced [20,21]:

$$r_c = \sigma_1^{\text{ampl}} / 2\sigma'_3 \quad (1)$$

$$R_c = \sigma_3^{\text{ampl}} / 2\sigma'_3 \quad (2)$$

where  $\sigma_1^{\text{ampl}}$ ,  $\sigma_3^{\text{ampl}}$  represents the amplitude of cyclic axial stress and lateral stress, respectively,  $\sigma'_3$  represents the effective lateral stress after consolidation. Since the maximum application frequency of bidirectional coupling of the test instrument is 5 Hz, and the vibration frequency of cyclic axial stress and cyclic confining pressure cannot be controlled independently during the test, a higher vibration frequency will cause the waveform of cyclic confining pressure to be unstable, which will have a certain impact on the test results. Therefore, based on the above considerations, the frequency of bidirectional cyclic vibration is set to be the same, and it is proposed to apply three frequencies during the test: 0.2 Hz, 0.5 Hz, 1.0 Hz.

### 3. Analysis of Test Results

#### 3.1. Comparison of Single and Bidirectional Cyclic Vibration for Different Frequencies

The hysteresis loop mainly reflects the deformation characteristics of the sample, stiffness degradation, and energy dissipation of the specimen under repeated cyclic loading, which is the basis for determining the restoring force model and nonlinear seismic response analysis [22–24]. Under the condition of unidirectional and bidirectional vibration, three groups of hysteretic curves with different vibration cycles at different frequencies are selected for comparison, as shown in Figures 5 and 6.

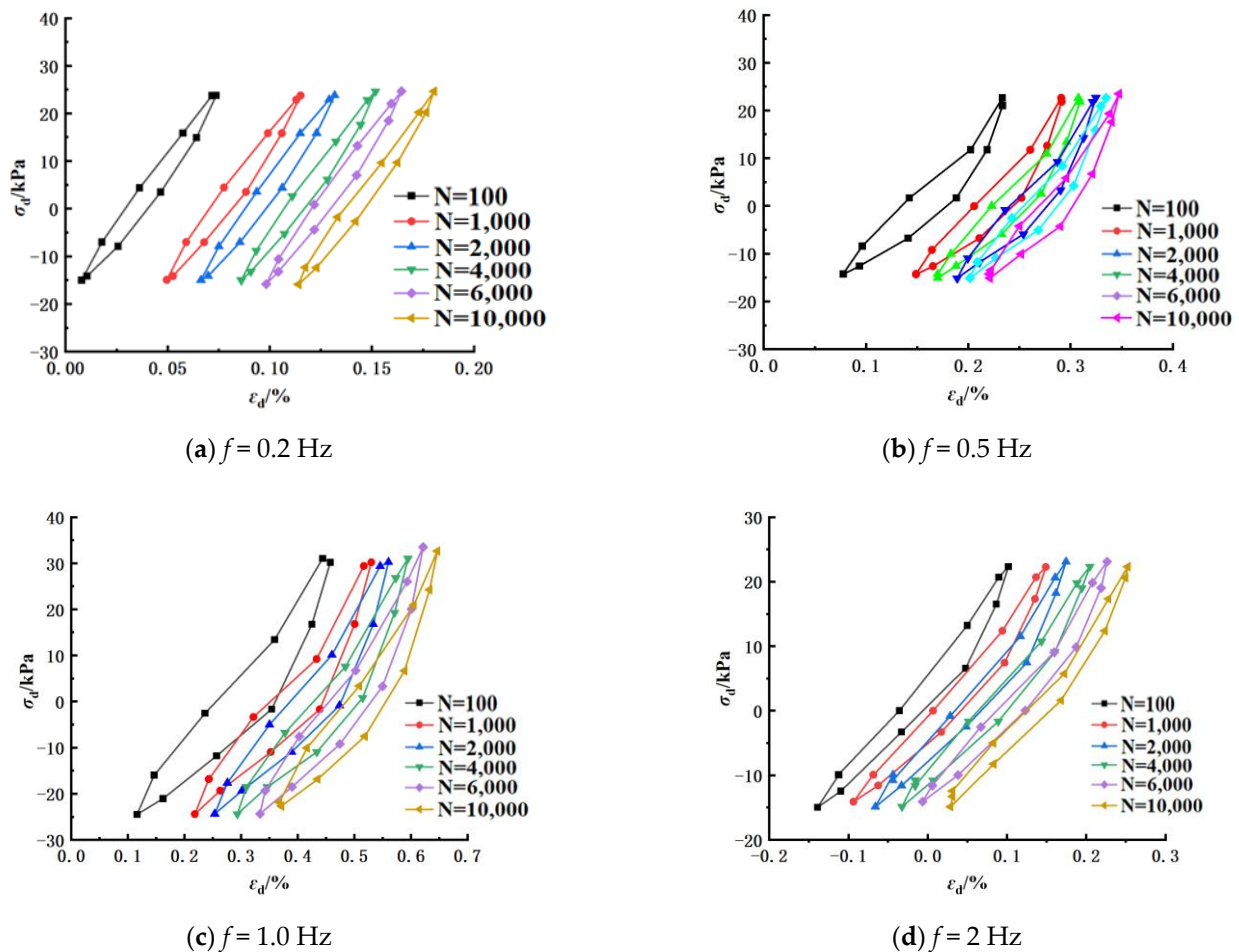


**Figure 5.** Hysteresis loops for different frequencies under unidirectional cyclic loading.

Through the comparison of hysteretic cycles with different frequencies under the condition of unidirectional and bidirectional vibration, it can be found that under the condition of unidirectional and bidirectional cyclic vibration, with the increase in frequency, the area of the hysteretic cycle tends to decrease; however, the slope of the connecting line at both ends of the hysteretic cycle tends to increase, indicating that with the increase in frequency, the soft clay with interlayer sand does not have enough time to deform and stretch. Therefore, the sample is constantly compacted, and the deformation rate decreases with the increase in frequency. For the same frequency, the area of bidirectional vibration hysteresis loop is smaller than that of unidirectional vibration hysteresis loop. The slope of the connecting line between the two ends of the bidirectional vibration hysteresis loop curve is less than that of the unidirectional vibration hysteresis loop curve.

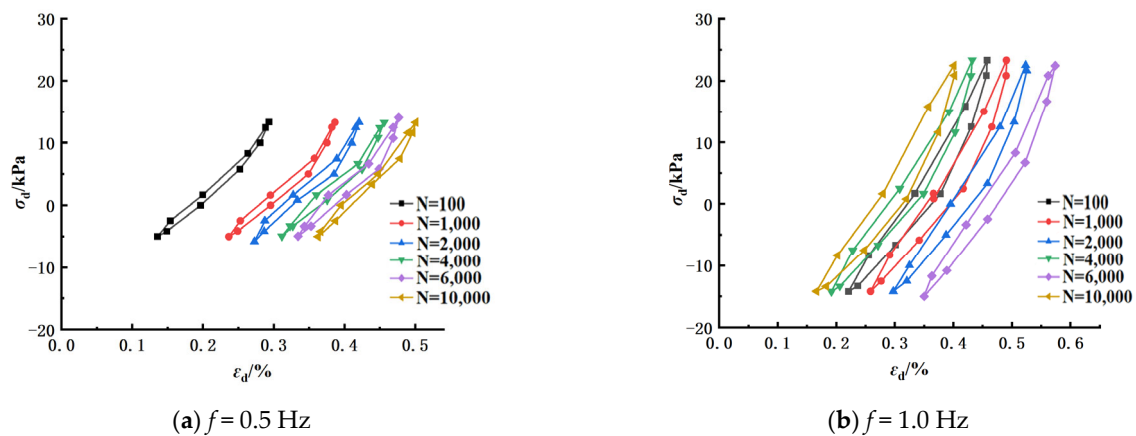


**Figure 6.** Hysteresis loops for different frequencies under bidirectional cyclic loading.

Figure 7 shows the effective stress path curve of the sandwich sand soft clay under different vibration frequencies. It can be seen from the figure that when the vibration frequency is 0.5–1.0 Hz, with the increase in the vibration frequency, the amplitude of the stress path of the cyclic vibration of the sample gradually increases from right to left, which is caused by the increase in the internal pore pressure and the acceleration of the average effective stress attenuation of the soil under the low-frequency load. When the vibration frequency is 2.0–5.0 Hz, the average effective stress attenuation slows down. In addition, under the action of a low-frequency load, the deviator stress of the sample does not attenuate; under a high-frequency cyclic load, the deviator stress reaches the peak at the initial moment and the deviator stress attenuates with the increase in the number of vibration cycles. At the same time, it can be seen from the figure that the stress path under different vibration frequencies is under the effective stress path  $K'_f$  of static load, and with the increase in vibration frequency, the stress path under cyclic load gradually approaches the  $K'_f$  line.

Figure 8 shows that when the cyclic stress ratio  $r_c = 0.225$ , the vibration frequency change in the load affects the influence of  $\varepsilon_d-N$  relationship curve. It can be seen from the figure that the vibration frequency also has a significant impact on the dynamic strain of soft clay. When the number of cycles is the same, the dynamic strain of the soil sample decreases gradually with the increase in vibration frequency. This is mainly because with the increase in frequency, the pore pressure of saturated interbedded sand and soft clay cannot rise in time, resulting in the failure of soil samples under a large number of cycles. In addition, the figure also shows that the magnitude of vibration frequency has little influence on the dynamic strain of saturated soft clay with sand interlayer. From the variation trend of the driven strain, it can be concluded that the critical cyclic stress ratio of saturated intercalated sand and soft clay will increase when the cyclic load frequency is large, while the critical cyclic stress ratio of saturated intercalated sand and soft clay will decrease when the cyclic load frequency is low.

Figure 9 shows the relationship between the dynamic pore pressure ratio  $u/p'_0$  and the number of cycles under different loading frequencies when the cyclic stress ratio  $r_c = 0.225$ . It can be seen from the figure that under the same load action times, the smaller the frequency of the soil sample, the greater the pore pressure, and the smaller the number of cycles, the failure will occur. The main reason for this phenomenon is that the pore water pressure has enough time to rise under the low-frequency cyclic load. However, under the cyclic load with high frequency, due to the existence of sand interlayer in the sample, the sand interlayer has the effect of water resistance and permeability reduction on the pore water in the soil sample, resulting in the pore water pressure rising in time. When the load frequency is 5 Hz, after 5000 cycles, the pore pressure develops slowly, and the pore pressure change mode is significantly different from the load frequency of 0.5 Hz and 1.0 Hz.

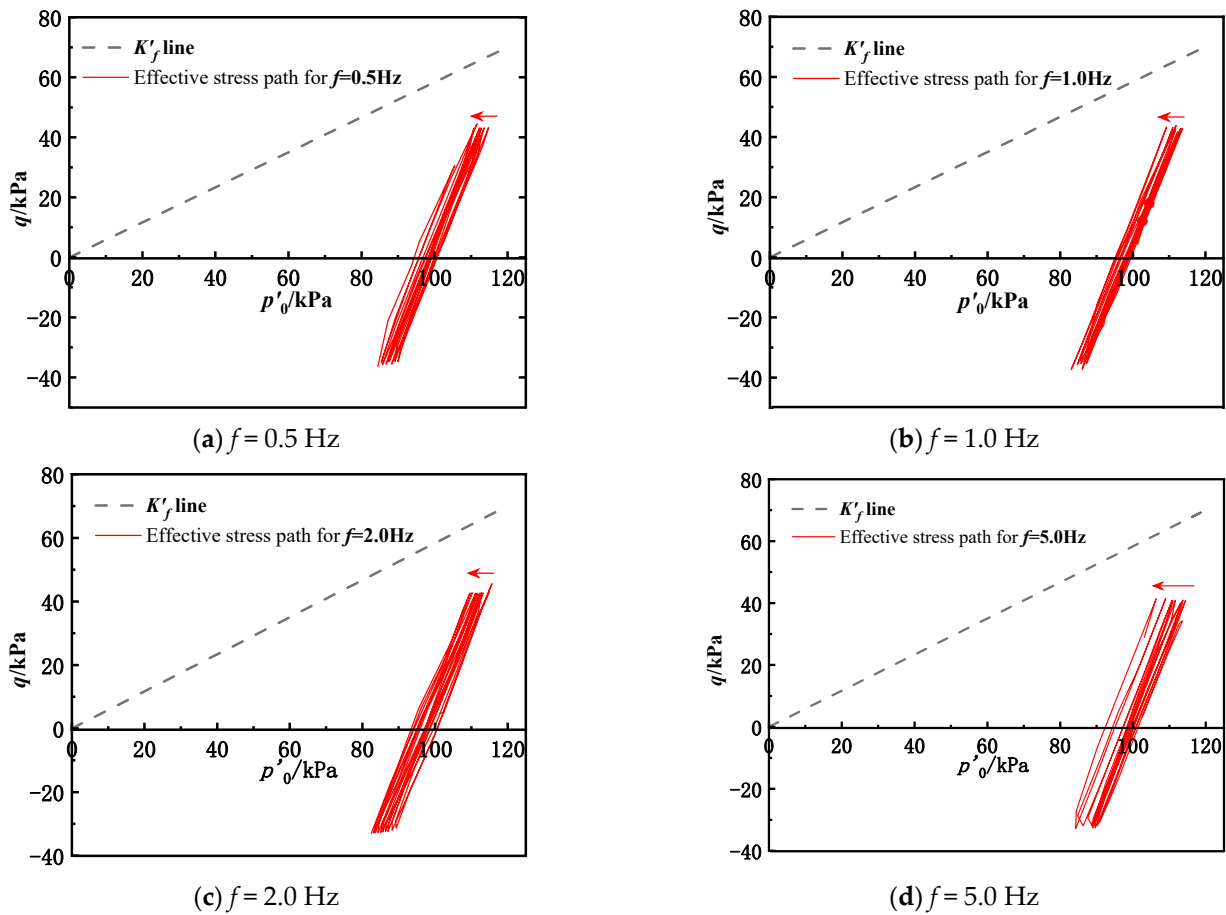


Figure 7. Effective stress path curve of sandwich sand soft clay under different frequencies.

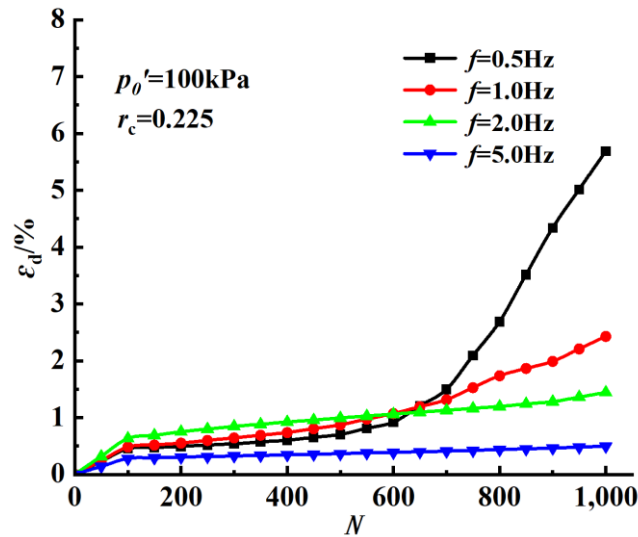


Figure 8. Double-amplitude dynamic strain of soil samples with cycles for different frequencies.

Figure 10 shows the change curve of shear modulus and damping ratio of soil samples with frequency. It can be seen from Figure 10a that under different cycles, the dynamic shear modulus of the sample gradually attenuates with the increase in load frequency. At the same time, under the same load frequency, the dynamic shear modulus of the sample tends to increase with the increase in the number of cyclic vibration, and the increase amplitude of the dynamic shear modulus increases with the increase in the number of

cycles at  $f = 0.5$  Hz. It can be seen from Figure 10b that the damping ratio of sandwich sand and soft clay shows the same change rule, and increases with the increase in load frequency, and under the same load frequency, the energy consumed by the soil sample to resist deformation increases with the increase in the number of cycles.

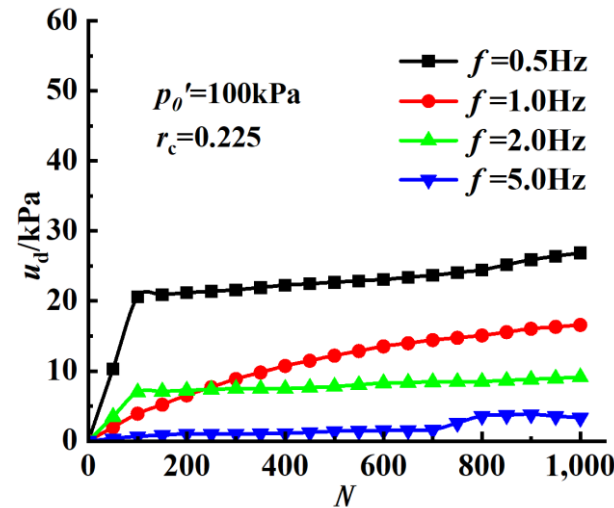
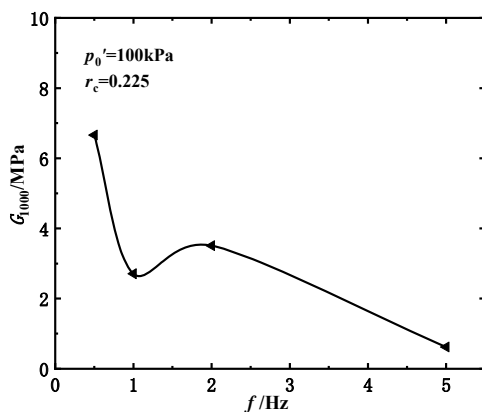
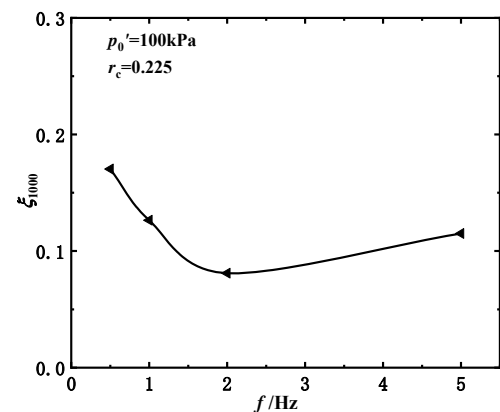


Figure 9. Dynamic pore pressure ratio of soil samples with cycles for different frequencies.



(a) Curve of shear modulus versus frequency



(b) Curve of damping ratio versus frequency

Figure 10. Variation of shear modulus and damping ratio with frequency.

### 3.2. Dynamic Characteristics of Soft Clay under Unidirectional and Bidirectional Cyclic Vibration

According to the test scheme (Table 2), the dynamic triaxial tests under different cyclic vibration conditions are carried out, and the relationship curves of the cumulative axial deformation, damping ratio, dynamic elastic modulus, and dynamic pore water pressure of saturated sandwich sand soft clay samples with the development of vibration times are obtained, as shown in Figure 11.

As shown in Figure 11a, under the same confining pressure, the specimen is subjected to static deviating stress during unidirectional vibration, which makes the cumulative axial deformation of the specimen develop rapidly at the initial stage of vibration. With the increase in vibration cycles, the growth of cumulative axial deformation slows down, and the change range of cumulative axial deformation caused by unidirectional vibration with the increase in frequency is greater than that of bidirectional vibration. Under the same dynamic stress ratio, the cumulative axial deformation caused by unidirectional and bidirectional vibration increases with the increase in frequency. This is because the normalized pore pressure increases with the increase in frequency under unidirectional

and bidirectional cycles, which reduces the normalized effective stress accordingly so that the cumulative axial deformation increases.

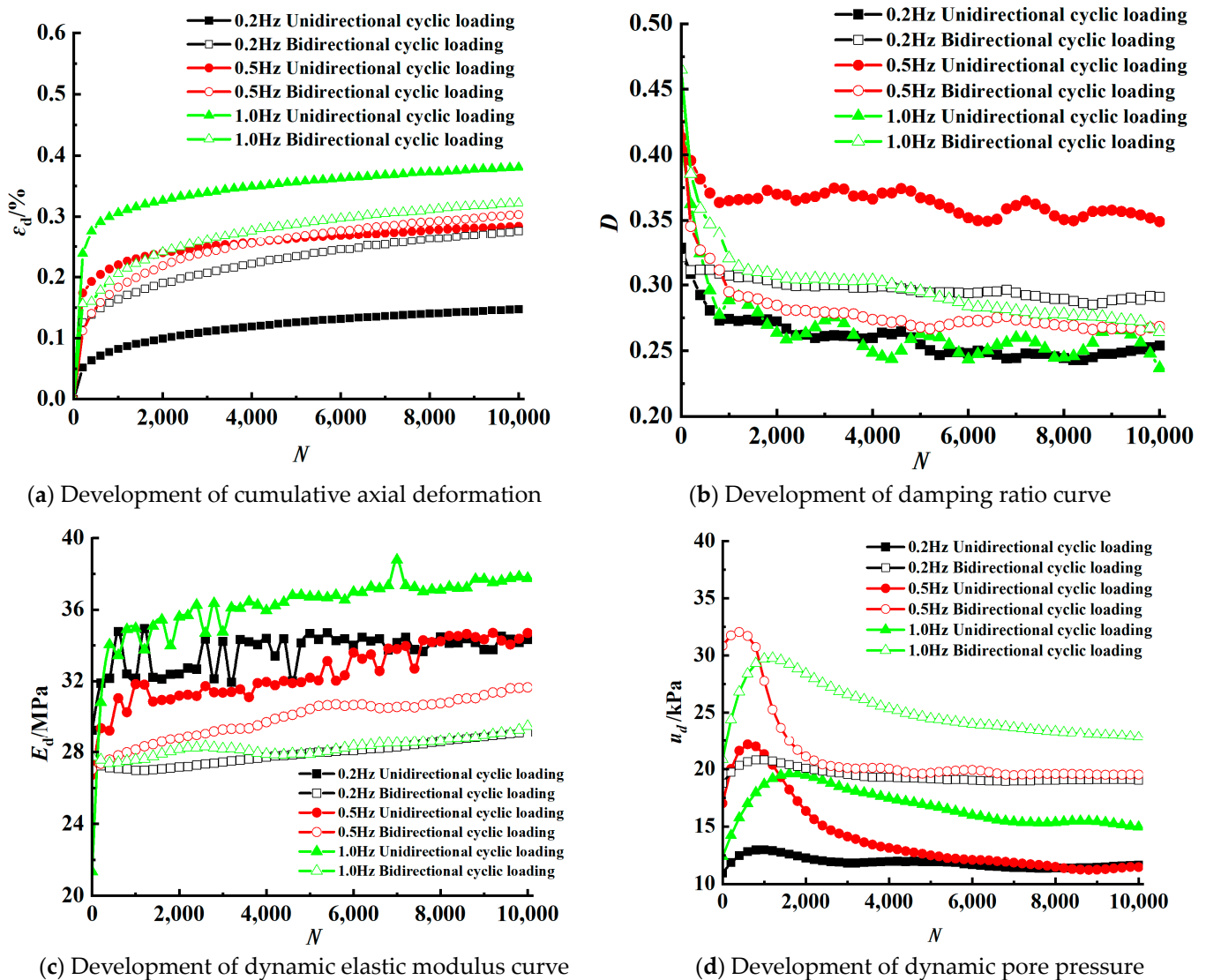


Figure 11. Development curve of dynamic parameters with vibration times.

As shown in Figure 11b, under unidirectional vibration, the damping ratio for the same axial dynamic stress ratio and different frequencies decreases with the increase in vibration times, the damping ratio of the first 2000 cycles decreases sharply, and the rate of decline of damping ratio decreases with the increase in vibration cycles. In addition, the greater the frequency, the faster the rate of decline of the damping ratio. In the case of bidirectional vibration, the rate of decline of the damping ratio is basically the same at different frequencies, and the amplitude of decline of the damping ratio is roughly the same.

As shown in Figure 11c, under unidirectional vibration, the dynamic elastic modulus of the sample with different frequencies develops rapidly at the initial stage of vibration, and the growth rate gradually slows down with the increase in the number of vibrations. This is because the soil body bears repeated cyclic loads under the amplitude, and the internal structure of the soil body has not changed significantly. Under bidirectional vibration, the dynamic elastic modulus changes in a small range and reaches the maximum value when  $f = 0.2$  Hz.

As shown in Figure 11d, under the condition of unidirectional vibration, the dynamic pore pressure increases with the increase in vibration frequency, and the dynamic pore pressure reaches the peak at the vibration number  $N = 1000$  and gradually tends to be flat with the increase in vibration number. Under the condition of bidirectional vibration, when the vibration times are less than 1000, the pore pressure of  $f = 0.5$  Hz develops faster than that of other frequencies.

Therefore, when the sample is subjected to dynamic load, different vibration modes have complex effects on the dynamic characteristics of the sample. The initial static deviator stress of unidirectional vibration will promote the development of cumulative plastic strain, and the tensile stress produced by bidirectional vibration will hinder the development of dynamic elastic modulus.

### 3.3. Dynamic Elastic Modulus and Damping Ratio under Different Vibration Times

The relationship curve between dynamic elastic modulus and frequency under different vibration cycle conditions is shown in Figure 12. Under the same axial dynamic stress ratio, the dynamic elastic modulus of unidirectional vibration decreases first and then increases with the increase in frequency. When  $f < 0.5$  Hz, the strength of the soft clay is significantly reduced by sand interlayer, and the energy consumption inside the soil increases with the increase in frequency, and reaches the peak value when  $f = 0.5$  Hz. For the same frequency, the dynamic elastic modulus of the sample increases with the increase in the number of vibrations. Under the condition of the same axial cyclic stress ratio and radial cyclic stress ratio, the dynamic elastic modulus of bidirectional vibration shows a change trend of first increasing and then decreasing with the increase in frequency, which is just opposite to the unidirectional vibration, indicating that the radial cyclic stress during bidirectional vibration enhances the ability of soil to resist deformation. Therefore, it can be concluded that when  $f < 0.5$  Hz, the sand interlayer can strengthen the strength of the soft clay, the dynamic elastic modulus increases with the increase in vibration times.

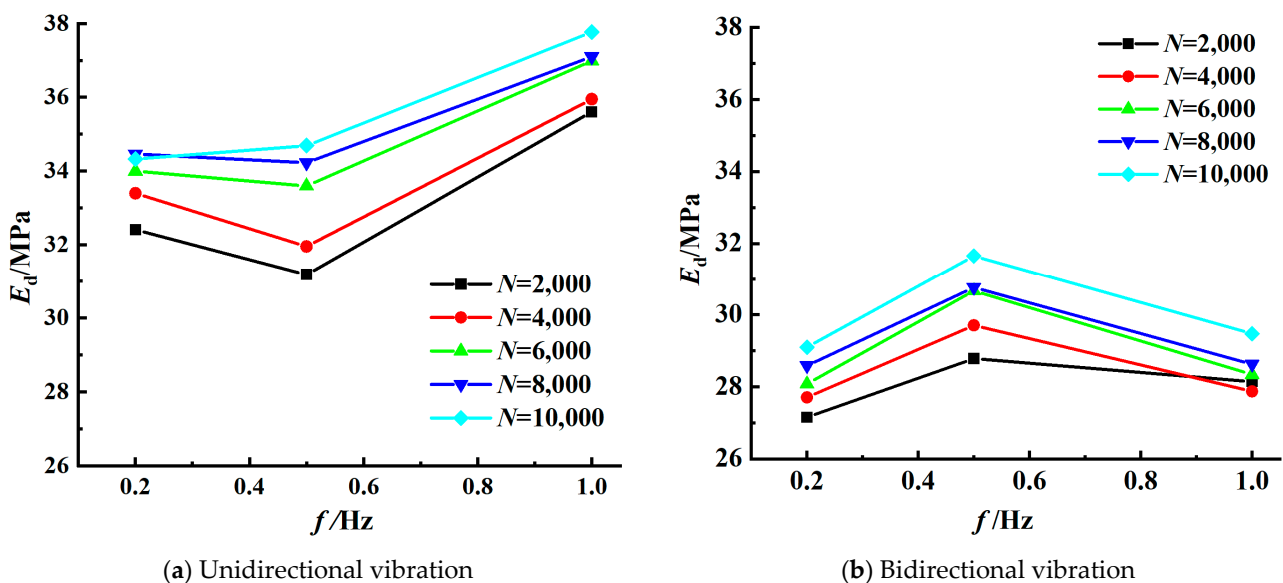


Figure 12. Variation of dynamic elastic modulus with frequency.

The relationship curve between damping ratio and frequency under different vibration cycle conditions is shown in Figure 13. It can be seen that under the same axial dynamic stress ratio, the damping ratio of unidirectional vibration increases first and then decreases with the increase in frequency, and reaches the maximum value when  $f = 0.5$  Hz. Under the same axial cyclic stress ratio and radial cyclic stress ratio, due to the action of lateral cyclic dynamic stress, the damping ratio of bidirectional vibration shows a trend of first decreasing and then slowly increasing with the increase in frequency. Therefore, it can be

concluded that under different cyclic loads, the change in frequency has a great impact on the saturated soft clay containing sand interlayer.

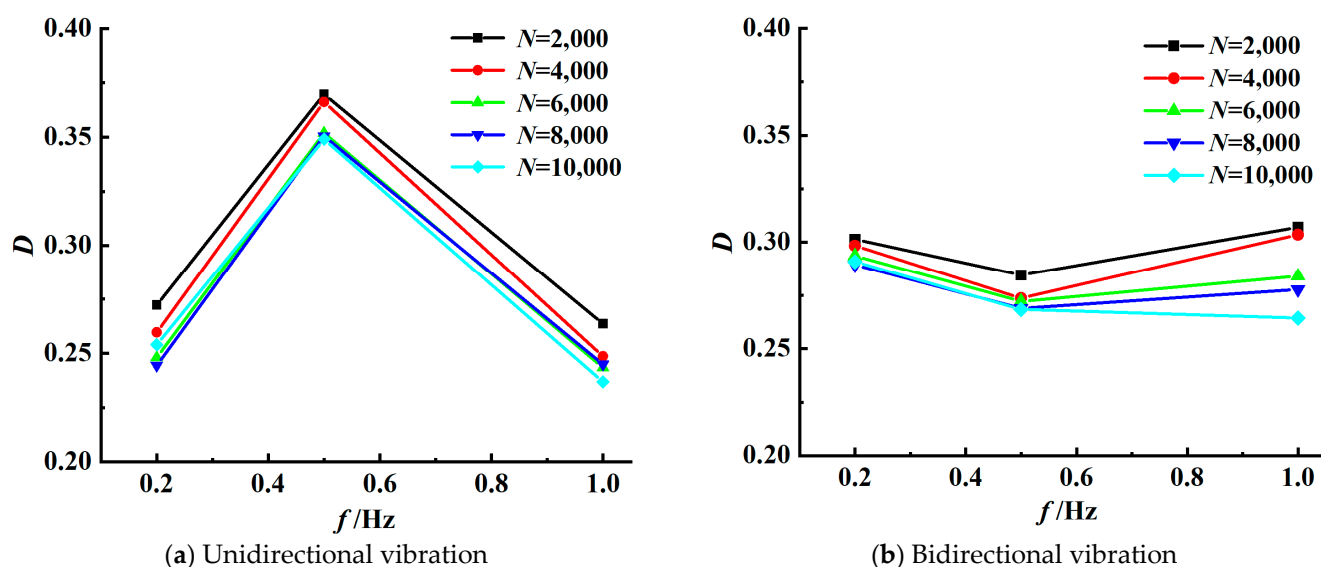


Figure 13. Variation of damping ratio with frequency.

#### 4. Conclusions

A large number of dynamic triaxial tests were conducted and the effects of frequency, stress ratio on shear modulus, and damping ratio were studied. The following conclusions can be drawn:

- (1) Under the condition of unidirectional and bidirectional cyclic vibration, the area of the hysteresis loop tends to decrease with the increase in frequency, and the slope of the connecting line at both ends of the hysteresis loop tends to increase. For the same frequency, the area of the bidirectional vibration hysteresis loop and the slope of the connecting line at both ends are smaller than that of the unidirectional cyclic vibration.
- (2) Under the same dynamic stress ratio, the cumulative axial deformation caused by unidirectional and bidirectional vibration increases with the increasing of frequency. Under the same cycle, the dynamic pore pressure increases with the increase in vibration frequency, and the dynamic pore pressure reaches the peak at the cycle  $N = 1000$ , and gradually tends to be flat with the increase in cycle.
- (3) For the same frequency, the dynamic elastic modulus of the sample increases with the increase in cycles, and the damping ratio decreases, and reaches the maximum value when  $f = 0.5$  Hz. Due to the effect of radial cyclic stress, the curves of dynamic elastic modulus and damping ratio with frequency under bidirectional vibration are just opposite to those under unidirectional vibration, indicating that radial cyclic stress can enhance the ability of soil samples to resist deformation.

**Author Contributions:** Conceptualization, S.W., Y.C., L.Z., Y.P. and B.C.; methodology, S.W., Y.C., L.Z., Y.P., B.C. and P.Z.; formal analysis, Y.C.; data curation, S.W. and P.Z.; writing—original draft preparation, S.W. and Y.F.; writing—review and editing, S.W. and Y.C. All authors have read and agreed to the published version of the manuscript.

**Funding:** The work presented in this paper was sponsored by the Supported by Systematic Project of Key Laboratory of New Technology for Construction of Cities in Mountain Area (No. LNTCCMA-20200104), the Systematic Project of Guangxi Key Laboratory of Disaster Prevention and Structural Safety (No. 2019ZDK005), the Initial Scientific Research Fund of Young Teachers in Ningbo University of technology (2019A610394), the Ningbo Public Welfare Science and Technology Planning Project (No. 2019C50012). These financial supports are gratefully acknowledged.

**Data Availability Statement:** The data used to support the findings of this study are included in the article.

**Conflicts of Interest:** The authors declare no conflict of interest.

## References

1. Qian, J.-G.; Du, Z.-B.; Yin, Z.-Y. Cyclic degradation and non-coaxiality of soft clay subjected to pure rotation of principal stress directions. *Acta Geotech.* **2017**, *13*, 943–959. [[CrossRef](#)]
2. Guo, L.; Chen, J.; Wang, J.; Cai, Y.; Deng, P. Influences of stress magnitude and loading frequency on cyclic behavior of K0-consolidated marine clay involving principal stress rotation. *Soil Dyn. Earthq. Eng.* **2016**, *84*, 94–107. [[CrossRef](#)]
3. Qian, J.-G.; Wang, Y.-G.; Yin, Z.-Y.; Huang, M.-S. Experimental identification of plastic shakedown behavior of saturated clay subjected to traffic loading with principal stress rotation. *Eng. Geol.* **2016**, *214*, 29–42. [[CrossRef](#)]
4. Guo, L.; Wang, J.; Cai, Y.; Liu, H.; Gao, Y.; Sun, H. Undrained deformation behavior of saturated soft clay under long-term cyclic loading. *Soil Dyn. Earthq. Eng.* **2013**, *50*, 28–37. [[CrossRef](#)]
5. France, J.W.; Sangrey, D.A. Effects of Drainage in Repeated Loading of Clays. *J. Geotech. Eng. Div.* **1977**, *103*, 769–785. [[CrossRef](#)]
6. Talesnick, M.; Frydman, S. Irrecoverable and Overall Strains in Cyclic Shear of Soft Clay. *Soils Found.* **1992**, *32*, 47–60. [[CrossRef](#)] [[PubMed](#)]
7. Andersen, K.H.; Brown, S.F.; Foss, I.; Poul, J.H.; Rosenbrand, W.F. Effect of cyclic loading on clay behavior. In Proceedings of the Design and Construction of Offshore Structures, London, UK, 7 July 2015; pp. 75–79.
8. Yasuhara, K.; Murakami, S.; Song, B.-W.; Yokokawa, S.; Hyde, A.F.L. Postcyclic Degradation of Strength and Stiffness for Low Plasticity Silt. *J. Geotech. Geoenvironmental Eng.* **2003**, *129*, 756–769. [[CrossRef](#)]
9. Matsui, T.; Bahr, M.; Abe, N. Estimation of shear characteristic degradation and stress-stain relationship of saturated clay after cyclic loading. *Soil Found.* **1992**, *32*, 161–172.
10. Kavvadas, M.; Amorosi, A. A constitutive model for structured soils. *Géotechnique* **2000**, *50*, 263–273.
11. Savvides, A.A.; Papadarakakis, M. A computational study on the uncertainty quantification of failure of clays with a modified Cam-Clay yield criterion. *SN Appl. Sci.* **2021**, *3*, 659.
12. Seed, H.B.; Lee, K.L. Liquefaction of Saturated Sand during Cyclic Loading. *J. Soil Mech. Found. Div. ASCE* **1966**, *92*, 105–134. [[CrossRef](#)]
13. Wichtmann, T.; Niemunis, A.; Triantafyllidis, T. On the influence of the polarization and the shape of the strain loop on strain accumulation in sand under high-cyclic loading. *Soil Dyn. Earthq. Eng.* **2007**, *27*, 14–28. [[CrossRef](#)]
14. Kammerer, A.M.; Seed, B.; Wu, J. Pore water development in liquefiable soils under bi-directional loading conditions. In Proceedings of the 13th World Conference on Earthquake Engineering, Vancouver, BC, Canada, 1–6 August 2004; pp. 697–704.
15. Hyde, A.F.L.; Ward, S.J. Effect of cyclic loading on the undrained shear strength of a silty clay. *Mar. Geotechnol.* **1986**, *6*, 299–314. [[CrossRef](#)]
16. Silvestri, V.; Bouteldja, M. On the consolidation response of a sensitive clay under cyclic loading. In Proceedings of the Canadian Geotechnical Conference, Saskatoon, SK, Canada, 27–29 September 1993; pp. 455–464.
17. Narasimha, R.S. Behaviour of marine clay under wave type of cyclic loading. In Proceedings of the International Conference on Off-shore Mechanics and Arctic Engineering-OMAE, Cancun, Mexico, 8–13 June 2003.
18. Liang, R.Y.; Ma, F. Anisotropic Plasticity Model for Undrained Cyclic Behavior of Clays. I: Theory. *J. Geotech. Eng.* **1992**, *118*, 229–245. [[CrossRef](#)]
19. Rehman, Z.U.; Khalid, U.; Ijaz, N.; Mujtaba, H.; Haider, A.; Farooq, K.; Ijaz, Z. Machine learning-based intelligent modeling of hydraulic conductivity of sandy soils considering a wide range of grain sizes. *Eng. Geol.* **2022**, *311*, 106899. [[CrossRef](#)]
20. Cai, Y.; Gu, C.; Wang, J.; Juang, C.H.; Xu, C.; Hu, X. One-Way Cyclic Triaxial Behavior of Saturated Clay: Comparison between Constant and Variable Confining Pressure. *J. Geotech. Geoenvironmental Eng.* **2013**, *139*, 797–809. [[CrossRef](#)]
21. Idriss, I.M.; Dobry, R.; Singh, R.D. Nonlinear Behavior of Soft Clays during Cyclic Loading. *J. Geotech. Eng. Div.* **1978**, *104*, 1427–1447. [[CrossRef](#)]
22. Rehman, Z.U.; Luo, F.; Wang, T.; Zhang, G. Large-Scale Test Study on the Three-Dimensional Behavior of the Gravel–Concrete Interface of a CFR Dam. *Int. J. Géoméch.* **2020**, *20*, 04020046. [[CrossRef](#)]
23. Rehman, Z.U.; Zhang, G. Cyclic behavior of gravel–steel interface under varying rotational shear paths. *Can. Geotech. J.* **2021**, *58*, 305–316. [[CrossRef](#)]
24. Rehman, Z.U.; Zhang, G. Shear coupling effect of monotonic and cyclic behavior of the interface between steel and gravel. *Can. Geotech. J.* **2018**, *56*, 876–884. [[CrossRef](#)]

**Disclaimer/Publisher’s Note:** The statements, opinions and data contained in all publications are solely those of the individual author(s) and contributor(s) and not of MDPI and/or the editor(s). MDPI and/or the editor(s) disclaim responsibility for any injury to people or property resulting from any ideas, methods, instructions or products referred to in the content.